

A magnesiothermic reaction process for the scalable production of mesoporous silicon for rechargeable lithium batteries†

Cite this: *Chem. Commun.*, 2013, **49**, 6743

Received 27th April 2013,
Accepted 6th June 2013

DOI: 10.1039/c3cc43134g

www.rsc.org/chemcomm

An Xing,^a Jing Zhang,^b Zhihao Bao,^{*a} Yongfeng Mei,^b Ari S. Gordin^c and Kenneth H. Sandhage^c

Mesoporous, 3-D, nanocrystalline Si has been synthesized via the magnesiothermic reduction of SiO particles at a peak temperature of only 500 °C in a scalable flow-through reactor setup. Such 3-D porous Si as an anode material exhibited high, reversible capacities (i.e., >900 mA h g⁻¹ after 160 charge–discharge cycles at 1000 mA g⁻¹).

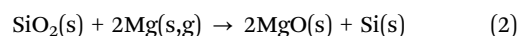
Silicon has attracted considerable interest as a high energy density and relatively safe anode material for lithium ion batteries, owing to its high theoretical specific capacity (4200 mA h g⁻¹) and moderate electrochemical potential versus Li/Li⁺ compared to graphite.¹ However, large volume changes (>300%) upon lithiation–delithiation of silicon during electrochemical cycling can lead to pulverization and disintegration of silicon anodes, and a rapid reduction in capacity.¹ Porous nanostructured silicon assemblies have been found to be more accommodating towards such volume changes and have exhibited significantly improved cyclic performance.² Moreover, such porous structures can present large accessible surface areas to liquid electrolytes and facilitate fast transport of Li ions for excellent rate properties. The synthesis of highly-porous 3-D nanocrystalline Si from various forms of biogenic and synthetic amorphous SiO₂ has been accomplished by several authors through the use of a patented magnesiothermic reaction process.³ This process has previously been conducted with magnesium vapor in sealed containers at elevated temperatures (typically at or above 650 °C, the melting point of Mg).³ Although it has been reported that nanosized silicon was reduced from SiO with Mg by mechanochemical reduction,⁴ the use of a less stable form of oxidized silicon as a reactant to allow for lower-temperature magnesiothermic reduction in a flowing inert atmosphere has not been examined.

Here, we demonstrate that solid silicon monoxide, SiO, can be converted into highly-porous Si via magnesiothermic reduction at only 500 °C (i.e., well below the melting point of Mg). At such a modest temperature, the reaction could be conducted with a solid mixture of SiO and Mg powders in a flowing, non-combustible H₂–Ar mixture within a tube furnace (i.e., in a readily scalable configuration) without appreciable magnesium vapor loss. After removal of the Mg-bearing products via selective acid dissolution, a highly mesoporous, interconnected 3-D network of nanocrystalline (~10 nm) Si was generated. Such porous Si as anodes exhibited high, reversible capacities (i.e., >900 mA h g⁻¹ after 160 charge–discharge cycles at 1000 mA g⁻¹).

The solid brown amorphous SiO powder (Fig. S1 and S2, ESI†) was allowed to undergo the following reaction with Mg at a peak temperature of 500 °C:



The Gibbs free energy change, ΔG , for this reaction, is -383.5 kJ (per mole of SiO consumed) at 500 °C. This value is more negative than the ΔG value of -339.6 kJ (per mole of SiO₂ consumed) obtained for the following reaction with amorphous SiO₂:^{5a-c}



A mixture of Mg(s) and SiO(s) containing a slight excess of Mg (Mg:SiO molar ratio of 1.1:1) was held at 300 °C for 3 h, and then at 500 °C for 1 or 12 h, within a flowing 5% H₂–95% Ar (non-combustive) gas atmosphere. X-ray diffraction (XRD) analysis of the products obtained after 1 h of reaction (Fig. 1a) revealed the presence of Mg₂Si along with Si and MgO. After 12 h of reaction, the intensities of diffraction peaks for the Mg₂Si phase decreased (and the half widths of these peaks increased) relative to diffraction peaks for Si and MgO (Fig. 1b), which was consistent with the consumption of some of the previously formed Mg₂Si. Little (<1%) weight change was detected between the starting Mg–SiO powder mixture and the MgO–Mg₂Si–Si mixture generated after 500 °C/12 h treatment. Hence, the significant loss of Mg₂Si between 1 and 12 h at 500 °C could not be attributed to the decomposition of Mg₂Si via the selective

^a Shanghai Key Laboratory of Special Artificial Microstructure Materials and Technology, School of Physics Science and Engineering, Tongji University, 1239 Siping Road, Shanghai 200092, China. E-mail: zbao@tongji.edu.cn; Fax: +86-21-65988060; Tel: +86-21-65988060

^b Department of Materials Science and Engineering, Fudan University, 220 Handan Road, Shanghai 200433, China

^c School of Materials Science and Engineering, Georgia Institute of Technology, 771 Ferst Drive, Atlanta, GA 30332, USA

† Electronic supplementary information (ESI) available. See DOI: 10.1039/c3cc43134g

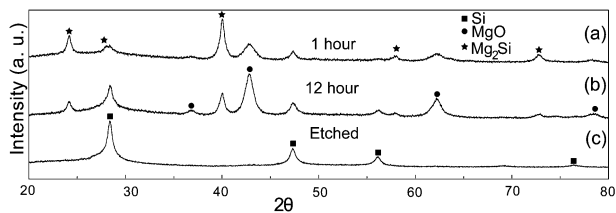
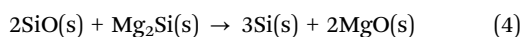
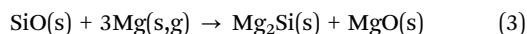


Fig. 1 XRD patterns obtained from products generated by the reaction of SiO and Mg at 500 °C: (a) for 1 h and (b) for 12 h. (c) XRD pattern obtained from the product generated by etching of the sample in (b) with an HCl solution and then an HF solution.

vaporization of Mg. Prior work has indicated that Mg₂Si can form as a transient intermediate phase *via* reaction (3), and then be consumed *via* reaction (4) to yield more Si and MgO:⁶



(Note: ΔG for reaction (3) is -456.0 kJ (per mole of SiO consumed) at 500 °C;^{5a-c} that is, reaction (3) was even more strongly favored than reaction (1)). The MgO and Mg₂Si products formed after 12 h of reaction at 500 °C were removed by selective acid dissolution, as revealed by energy-dispersive X-ray (EDX) analysis (Fig. S3a, ESI[†]), to yield a yellow-brown powder comprised of crystalline Si (Fig. 1c and Fig. S1, ESI[†]). Scherrer analysis of the XRD pattern yielded an average crystallite size of 10 nm for the Si product. The presence of fine Si nanocrystals was also confirmed using high resolution transmission electron microscopy (TEM, Fig. 2a). The surface area and pore size distribution of the Si product were evaluated *via* nitrogen adsorption–desorption analyses. The isothermal adsorption–desorption curve of the Si product (Fig. 2c) was of type IV with a H1 type hysteresis loop, which indicated that the Si product was largely mesoporous. BET and BJH analyses yielded values of 218.4 m² g⁻¹ and 0.274 cm³ g⁻¹ for the specific surface area and the specific mesopore volume, respectively, with a predominance of pores found to be below 10 nm in size (Fig. 2d).

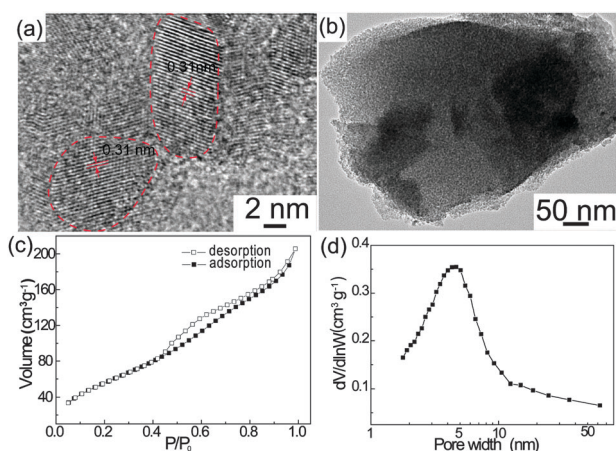


Fig. 2 (a and b) High and low magnification bright field TEM images, respectively, of porous Si prepared *via* reaction with Mg for 3 h at 300 °C and then 12 h at 500 °C, followed by acid dissolution of Mg-bearing product phases. (c) Isothermal nitrogen adsorption and desorption curves of the silicon product at 77 K. (d) Pore size distribution (from BJH analysis) of the porous silicon product.

Although the porous structure was not obvious in the secondary electron microscopy (SEM) image (Fig. S3b, ESI[†]) of the silicon product, a relatively high population of <10 nm pores was also evident from bright field TEM images of the Si product (Fig. 2b and Fig. S4, ESI[†]). Such mesoporosity was consistent with the average crystallite sizes of the MgO (8.2 nm) and Mg₂Si (13.4 nm) products, as determined by Scherrer analyses of the XRD pattern shown in Fig. 1b; that is, such mesoporosity was largely created by selective acid dissolution of the Mg-bearing product phases.

To evaluate the influence of the 300 °C/3 h treatment on the evolution of product phases, a mixture of Mg and SiO reactants with the same molar ratio (Mg:SiO molar ratio of 1.1:1) was directly heated at 2 °C min⁻¹ from room temperature to 500 °C (*i.e.*, no hold at 300 °C) and held at this temperature for 1 or 6 h. XRD analysis of the resulting products (Fig. S5a and b, ESI[†]) revealed relatively narrow Si diffraction peaks which, according to Scherrer analysis, corresponded to an average Si crystal size of 67 nm. Furthermore, unlike for the specimens that had first been exposed to the 300 °C/3 h treatment, diffraction peaks were not detected for Mg₂Si after 1 h at 500 °C (Fig. S5a, ESI[†]). This latter observation suggested that the rate of direct MgO–Si formation *via* reaction (1) was enhanced by continuous heating to 500 °C, whereas the use of the 300 °C treatment prior to reaction at 500 °C promoted the formation of Mg₂Si as an intermediate phase. After direct heating of the Mg–SiO mixture to 500 °C and reaction for 6 h, followed by selective acid etching of MgO, the Si product formed as a porous, interconnected matrix with a solid wall thickness of 50–150 nm, as revealed by the SEM and TEM images in Fig. S6a and S6c (ESI[†]), respectively. Appreciable macroporosity was detected, with most macropores possessing diameters of 50 to 300 nm (Fig. S6b, ESI[†]). BET and BJH analyses of these porous Si specimens yielded values of specific surface area and specific mesopore volume of only 5.4 m² g⁻¹ and 0.008 cm³ g⁻¹, respectively. High resolution TEM images (Fig. S6d, ESI[†]) revealed the presence of relatively large Si crystals, which was consistent with Scherrer analysis of the XRD pattern. Hence, the use of an intermediate 300 °C/3 h treatment, prior to reaction at 500 °C, yielded porous Si with much finer crystal size and with significantly higher specific surface area and specific mesopore volume.

For electrochemical evaluation, porous Si electrodes (prepared using the 300 °C/3 h and 500 °C/12 h treatments) with sodium alginate as a binder were cycled between 5 mV and 1 V in a solution of 1 M LiPF₆ with vinylene carbonate.^{2c,7} Plots of differential capacity (dQ/dV) versus voltage during the first three cycles are shown in Fig. 3a. The lithiation peaks at 0.21 V and 0.11 V have been associated with the formation of amorphous Li_xSi.⁸ However, a peak at 0.25 V, resulting from the formation of Li₄SiO₄ and Li₂O from SiO,⁹ was not observed, which was consistent with the absence of SiO after magnesiothermic reduction. The delithiation peaks at 0.28 V and 0.44 V have been ascribed to the phase transition between amorphous Li_xSi and amorphous Si.^{8,10} Representative galvanostatic charge–discharge profiles for electrodes containing porous Si (derived from SiO) at various current densities are shown in Fig. 3b. At 100 mA g⁻¹, the porous Si-bearing electrodes exhibited capacities of 2828.5 and 1737.2 mA h g⁻¹ for the discharge and charge cycles, respectively. This irreversible capacity loss may be attributed to the formation of a SEI layer on the electrode surface

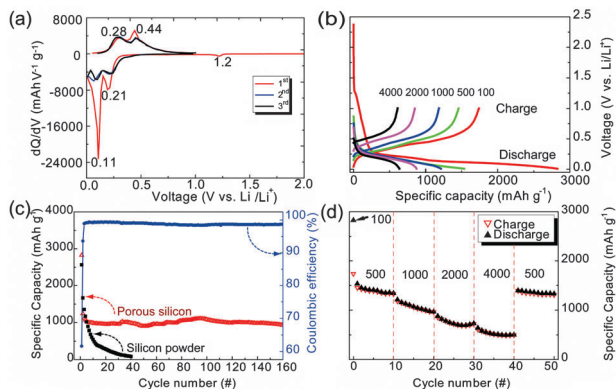


Fig. 3 (a) Plots of the differential capacity (dQ/dV) vs. voltage (V) for nanocrystalline Si-based electrodes (prepared *via* magnesiothermic reduction of SiO) for the first three cycles. (b) Representative voltage profiles of porous nanocrystalline Si-based electrodes at various current densities. (c) Cycling performance of solid Si powder and porous nanocrystalline Si-based electrodes. (d) Rate performance of porous nanocrystalline silicon-based electrodes.

and the consumption of some Li^+ due to other irreversible reactions. The cycling stability of anodes containing porous nanocrystalline Si (derived from SiO powder of $<2.5 \mu\text{m}$ size) was compared with that of anodes prepared with commercially-available dense Si powder ($<2.5 \mu\text{m}$ size). For the porous, nanocrystalline Si-bearing electrodes, a capacity of $923.5 \text{ mA h g}^{-1}$ (*i.e.*, 83.4% of the value after the second cycle) at 1000 mA g^{-1} was retained after 160 cycles, with the Coulombic efficiency reaching 98% even after just 3 cycles (Fig. 3c). While the dense Si particle-bearing electrodes exhibited an initial capacity of 3863 mA h g^{-1} at 100 mA g^{-1} , the capacity dropped to 86 mA h g^{-1} (lower than the theoretical capacity of graphite) after only 40 charge–discharge cycles at 1000 mA g^{-1} . The performance of porous nanocrystalline silicon is also superior to that of the macroporous silicon product (Fig. S7, ESI[†]) without the treatment at 300°C . SEM images of the Si in these electrodes before and after such cycling are shown in Fig. S8 (ESI[†]). After 160 cycles, the nanocrystalline, porous Si particles increased in their apparent size, presumably due to the formation of the SEI layer and irreversible expansion associated with swelling during lithiation. Nonetheless, the morphologies and apparent connectivity of these porous Si particles were retained after cycling. However, appreciable swelling and cracking were observed for the dense Si particles after just 40 charge–discharge cycles. The mesoporous, nanocrystalline Si particles were clearly better able to accommodate volume changes associated with repeated lithiation–delithiation. The rate capability of the porous nanocrystalline Si-based electrodes at various discharge rates is revealed in Fig. 3d. Reversible capacities of 1342.2 , 964.7 , 725.0 , and $493.1 \text{ mA h g}^{-1}$ were achieved at discharge rates of 500 , 1000 , 2000 , and 4000 mA g^{-1} , respectively. These values are higher by factors of 3.6, 2.6, 1.8, and 1.3 times, respectively, than the theoretical capacity of graphite (372 mA h g^{-1}).

The present work demonstrates that mesoporous, three-dimensionally-interconnected nanocrystalline Si can be synthesized from solid SiO *via* a magnesiothermic reaction process at a peak temperature of only 500°C (*i.e.*, well below the melting point of Mg). The present low-temperature conversion was conducted *via* reaction with a solid mixture of SiO and Mg

powders in a flowing, non-combustible H_2 –Ar mixture within a tube furnace (*i.e.*, in a readily-scalable configuration) without appreciable loss of Mg as vapor. When utilized as anodes for lithium ion batteries, the uniform network of mesopores interspersed within the 3-D interconnected nanocrystalline silicon acted to accommodate the volume expansion during the lithiation–delithiation process and enabled relatively rapid lithium ion transport and lithium incorporation into the nanocrystalline silicon for enhanced rate performance.

This work was supported by the Program for New Century Excellent Talents in University (No. NCET-10-0595), Key Basic Research Projects of Science and Technology Commission of Shanghai (No. 11JC1412900), Scientific Research Foundation for Returned Scholars, the Ministry of Education of China, and the National Science Foundation of China Program (No. 21271140). Support for ASG and KHS was provided by the U.S. Department of Energy, Office of Basic Energy Sciences, Award No. DE-SC0002245.

Notes and references

- (a) M. Winter, J. O. Besenhard, M. E. Spahr and P. Novak, *Adv. Mater.*, 1998, **10**, 725; (b) U. Kasavajjula, C. Wang and A. J. Appleby, *J. Power Sources*, 2007, **163**, 1003; (c) J. Cho, *J. Mater. Chem.*, 2010, **20**, 4009.
- (a) H. Wu, G. Chan, J. W. Choi, I. Ryu, Y. Yao, M. T. McDowell, S. W. Lee, A. Jackson, Y. Yang, L. B. Hu and Y. Cui, *Nat. Nanotechnol.*, 2012, **7**, 309; (b) M. Y. Ge, J. P. Rong, X. Fang and C. W. Zhou, *Nano Lett.*, 2012, **12**, 2318; (c) I. Kovalenko, B. Zdyrko, A. Magasinski, B. Hertzberg, Z. Milicev, R. Burtovoy, I. Luzinov and G. Yushin, *Science*, 2011, **333**, 75; (d) B. M. Bang, H. Kim, H. K. Song, J. Cho and S. Park, *Energy Environ. Sci.*, 2011, **4**, 5013; (e) A. Magasinski, P. Dixon, B. Hertzberg, A. Kvit, J. Ayala and G. Yushin, *Nat. Mater.*, 2010, **9**, 461; (f) L. F. Cui, Y. Yang, C. M. Hsu and Y. Cui, *Nano Lett.*, 2009, **9**, 3370; (g) M. H. Park, M. G. Kim, J. Joo, K. Kim, J. Kim, S. Ahn, Y. Cui and J. Cho, *Nano Lett.*, 2009, **9**, 3844; (h) C. K. Chan, H. L. Peng, G. Liu, K. McIlwrath, X. F. Zhang, R. A. Huggins and Y. Cui, *Nat. Nanotechnol.*, 2008, **3**, 31.
- (a) Z. H. Bao, M. R. Weatherspoon, S. Shian, Y. Cai, P. D. Graham, S. M. Allan, G. Ahmad, M. B. Dickerson, B. C. Church, Z. T. Kang, H. W. Abernathy, C. J. Summers, M. L. Liu and K. H. Sandhage, *Nature*, 2007, **446**, 172; (b) K. H. Sandhage and Z. Bao, *U.S. Patent*, 7,615,206, 2009; (c) Y. Yu, L. Gu, C. B. Zhu, S. Tsukimoto, P. A. van Aken and J. Maier, *Adv. Mater.*, 2010, **22**, 2247; (d) H. P. Jia, P. F. Gao, J. Yan, J. L. Wang, Y. N. Nuli and Z. Yang, *Adv. Energy Mater.*, 2011, **1**, 1036; (e) W. Chen, Z. L. Fan, A. Dhanabalan, C. H. Chen and C. L. Wang, *J. Electrochem. Soc.*, 2011, **158**, A1055; (f) X. Xin, X. F. Zhou, F. Wang, X. Y. Yao, X. X. Xu, Y. M. Zhu and Z. P. Liu, *J. Mater. Chem.*, 2012, **22**, 7724.
- W. Zhou, S. Upreti and S. Whittingham, *Electrochem. Commun.*, 2011, **13**, 1102.
- (a) I. Barin and G. Platzki, *Thermochemical Data of Pure Substances*, VCH Verlagsgesellschaft mbH, Weinheim, Germany, 1995; (b) S. M. Schnurre, J. Grosner and R. Schmid-Fetzer, *J. Non-Cryst. Solids*, 2004, **336**, 1; (c) K. V. Gourishankar, M. Karaminezhad Ranjbar and G. R. St. Pierre, *J. Phase Equilib.*, 1993, **14**, 601.
- E. Fueglein and U. Schubert, *Chem. Mater.*, 1999, **11**, 865.
- (a) Y. S. Hu, R. Demir-Cakan, M. M. Titirici, J. O. Muller, R. Schlogl, M. Antonietti and J. Maier, *Angew. Chem., Int. Ed.*, 2008, **47**, 1645; (b) V. Baranchugov, E. Markevich, E. Pollak, G. Salitra and D. Aurbach, *Electrochem. Commun.*, 2007, **9**, 796.
- (a) S. H. Nam, K. S. Kim, H.-S. Shim, S. H. Lee, G. Y. Jung and W. B. Kim, *Nano Lett.*, 2011, **11**, 3656; (b) H. Kim and J. Cho, *Nano Lett.*, 2008, **8**, 3688.
- T. Kim, S. Park and S. M. Oh, *Electrochem. Solid-State Lett.*, 2007, **154**, A1112.
- (a) M. N. Obrovac and L. Christensen, *Electrochem. Solid-State Lett.*, 2004, **7**, A93; (b) J. H. Ryu, J. W. Kim, Y. E. Sung and S. M. Oh, *Electrochem. Solid-State Lett.*, 2004, **7**, A306.